Blinking statistics of a molecular beacon triggered by end-denaturation of DNA

2005 J. Phys.: Condens. Matter 17 S4305

(http://iopscience.iop.org/0953-8984/17/49/022)

INSTITUTE OF PHYSICS PUBLISHING JOURNAL OF PHYSICS: CONDENSED MATTER

J. Phys.: Condens. Matter **17** (2005) S4305–S4316 doi:10.1088/0953-8984/17/49/022

Blinking statistics of a molecular beacon triggered by end-denaturation of DNA

Tobias Ambjörnsson and Ralf Metzler

NORDITA—Nordic Institute for Theoretical Physics, Blegdamsvej 17, DK-2100 Copenhagen Ø, Denmark

E-mail: ambjorn@nordita.dk and metz@nordita.dk

Received 12 July 2005
Published 25 November 2005
Online at stacks.iop.org/JPhysCM/17/S4305

Abstract

We use a master equation approach based on the Poland–Scheraga free energy for DNA denaturation to investigate the (un)zipping dynamics of a denaturation wedge in a stretch of DNA that is clamped at one end. In particular, we quantify the blinking dynamics of a fluorophore–quencher pair mounted within the denaturation wedge. We also study the behavioural changes in the presence of proteins that selectively bind to single-stranded DNA. We show that such a set-up could be well suited as an easy-to-implement nanodevice for sensing environmental conditions in small volumes.

(Some figures in this article are in colour only in the electronic version)

1. Introduction

During the last decade or so, technical progress in detection and manipulation of single molecules and their dynamics has snowballed. By fluorescence spectroscopy, optical tweezers, atomic force microscopy, or patch clamp techniques, for instance, it is possible on the single-molecule level to probe the opening and closing dynamics of local denaturation zones in a DNA molecule [1], to study the binding of single-stranded DNA binding proteins to overstretched DNA [2, 3], to disrupt domains stepwise in a protein [4], and to monitor the passage of a biopolymer through a nanopore in a membrane [5, 6], to name just a few possibilities. This experimental progress is accompanied by advances in the theoretical understanding of fundamental processes relevant on small scales such as the Jarzinsky relation connecting measurements of the non-equilibrium work needed, e.g., to stretch an RNA segment [7] to the difference in the corresponding thermodynamic potential [8], and the entropy production along single trajectories exposed to stochastic forces [9]. Given the novel possibilities for synthesizing supramolecules with topologically confined mechanical units [10], entropy-based designer molecules such as molecular muscles were proposed [11, 12], and new possibilities for producing dynamic nanosensors discussed [13].

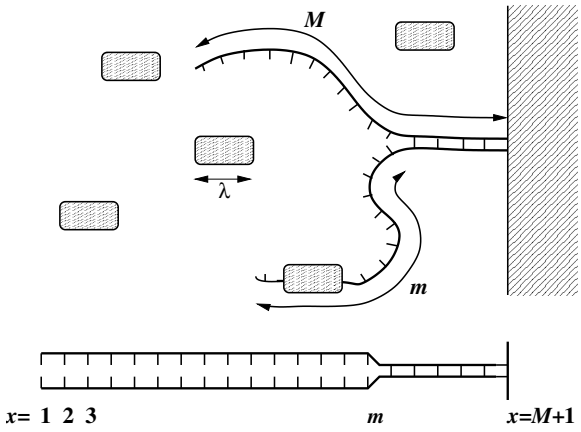

Figure 1. Schematic diagram of the end-denaturing of a double-stranded DNA molecule that is clamped at one end—here, by attachment to a wall. The number of denatured base-pairs is m, and the overall length of the DNA segment is M. Selectively single-stranded DNA binding proteins from the surrounding solution bind to the denatured portion of the DNA. Once bound, the SSBs lower the probability for closing of the denaturation wedge. In reality, the clamping can be achieved by sealing the denaturation zone created by AT base-pairs with a stretch of more stable GC base-pairs; compare [1].

In what follows, we explore the dynamics of a stretch of double-stranded DNA (dsDNA) that is clamped at one end but allowed to denature from the other, as sketched in figure 1. Internal bubble formation, in comparison, is suppressed by a Boltzmann factor $\sigma_0 \simeq 10^{-5} \ldots 10^{-3}$ [14], and this effect can therefore be neglected; see below. In the set-up we have in mind an individual base-pair is tagged with a fluorophore–quencher pair; see figure 2. Once separation has been achieved, the dye starts to fluoresce, and the resulting blinking can be detected [15]. Our aim is to establish a quantitative description of such a *molecular beacon*. We will use a master equation approach to describe the sequential unzipping and zipping dynamics of the denaturation wedge, also taking into account the possible presence of proteins that selectively bind to single-stranded DNA (ssDNA). These single-stranded DNA binding proteins (SSBs) occur in the cells of most organisms. Here, we show that the autocorrelation function for the blinking depends on the concentration of SSBs and the strength of binding between the single strand and the SSBs (the latter varies, for instance, with the salt concentration) as well as temperature. The denaturation wedge depicted in figure 2 therefore acts as a nanosensor that can be probed on the single-molecule level using fluorescence techniques.

2. Experimental set-up: quantifying the blinking dynamics of the molecular beacon

Before setting out to describe our general theoretical scheme, we first describe the experimental set-up we have in mind in some detail. We consider modelling the blinking behaviour of a fluorophore–quencher pair mounted on the denaturation wedge as shown in figure 2. This set-up, similar to the ones described in [1, 15], works as follows. As long as the dsDNA is intact, the fluorophore and quencher are in close proximity. Once they come apart from one another when the denaturation wedge opens up, the incident laser light causes fluorescence of the dye. The on/off blinking of this 'molecular beacon' can be monitored in the focus of a confocal microscope.

The blinking yields immediate information about the state of the base-pair that is tagged by the dye–quencher pair. Blinking, that is, indicates that the base-pair is currently broken. It

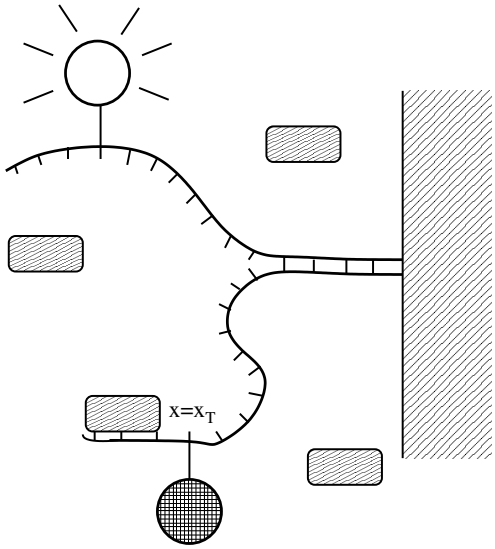

Figure 2. Schematic diagram of the molecular beacon set-up. A fluorophore starts to fluoresce in the incident laser light once the denaturation wedge moves the fluorophore apart from the quencher.

is therefore advantageous to define the random variable $I(t)$ with the property

$$I(t) = \begin{cases} 0 & \text{if base-pair at } x = x_T \text{ is closed} \\ 1 & \text{if base-pair at } x = x_T \text{ is open,} \end{cases} \tag{1}$$

and we are interested in the behaviour of the autocorrelation function

$$A(t) = \langle I(t)I(0)\rangle - \langle I\rangle_{\text{eq}}^2, \tag{2}$$

where $\langle I\rangle_{\text{eq}}$ is the (ensemble) equilibrium value. Given the fact that the formation of an internal denaturation bubble is connected with a rather high initiation barrier $\sigma_0 \simeq 10^{-5}\ldots 10^{-3}$ (corresponding to $7\ldots 12\ k_{\text{B}}T$ at room temperature), such bubbles are much less probable than denaturation from the unclamped end; we focus just on the end-denaturation. Therefore, a base-pair at $x = x_T$ is open if $m \geqslant x_T$; see figure 2. A word on the interpretation of the average $\langle I(t)I(0)\rangle$ is in order. Denoting by $\rho(I, t; I', 0)$ the associated joint probability density that the tagged base-pair is in state I at time t given that it was in state I' at initial time $t = 0$, we can rewrite the autocorrelation function as

$$\langle I(t)I(0)\rangle = \sum_{I,I'} I\rho(I, t; I', 0)I' = \rho(1, t; 1, 0). \tag{3}$$

This is nothing but the survival probability density for a denaturation wedge, i.e., the probability density for the base-pair being open at time t, given that is was open at $t = 0$.

In the remaining part of this study we present a general scheme for calculating the opening and closing dynamics for the physical system presented in figures 1 and 2. The focus is on presenting a scheme which allows for the calculation of the measurable quantity $A(t)$ defined above. We note, however, that our scheme is sufficiently general to allow for straightforward derivation of other experimental quantities, such as the binding dynamics of SSBs in optical tweezers overstretching set-ups [2, 3, 16]. In that case, the Boltzmann factor for opening a base-pair, $u = \exp(\beta\epsilon)$ (ϵ being the binding energy of a base-pair; see below), becomes

modified to $u = \exp(\beta\epsilon + \mathcal{T}\theta_0)$, where $\mathcal{T}$ is the external torque exerted by the optical tweezers set-up, and $\theta_0 = 2\pi/10.35$ is the relaxed dsDNA twist per base-pair.

3. Master equation for end-unzipping

Denote by $P(m, n, t)$ the probability distribution that there are m broken base-pairs and n bound SSBs at time t. As m and n are the slow variables of the system, their dynamics can be described in terms of the master equation

$$\begin{aligned}\frac{\partial P(m,n,t)}{\partial t} &= \mathsf{t}^+(m-1,n)P(m-1,n,t) + \mathsf{t}^-(m+1,n,t)P(m+1,n,t)\\ &\quad - [\mathsf{t}^+(m,n) + \mathsf{t}^-(m,n)]P(m,n,t)\\ &\quad + \mathsf{r}^+(m,n-1)P(m,n-1) + \mathsf{r}^-(m,n+1)P(m,n+1,t)\\ &\quad - [\mathsf{r}^+(m,n) + \mathsf{r}^-(m,n)]P(m,n,t); \end{aligned} \tag{4}$$

compare the discussion in [17–19]. With mediation by the transfer rates $\mathsf{t}^\pm$ and $\mathsf{r}^\pm$, the population of a given state (m, n) is continuously changed by (un)zipping a further base-pair and (un)binding an SSB. To complete the master equation (4), we need to specify the boundary conditions: the clamping to the right at base-pair $x = M + 1$ ensures that no further unzipping beyond base-pair M occurs, that is,

$$\mathsf{t}^+(M, n) = 0. \tag{5}$$

Moreover, if both branches of the denaturation wedge are fully occupied by SSBs, i.e., the maximum number of SSBs,

$$n^{\max}(m) = 2\left[\frac{m}{\lambda}\right], \tag{6}$$

is bound, then the base-pair at the zipping fork is not allowed to close:

$$\mathsf{t}^-\left(m = \frac{n\lambda}{2}, n = n^{\max}(m)\right) = 0. \tag{7}$$

Also, if only one of the two branches of the wedge is fully occupied, the zipper cannot close:

$$\mathsf{t}^-\left(m = \frac{(n+1)\lambda}{2}, n = n^{\max}(m) - 1\right) = 0. \tag{8}$$

Similarly to the case for (un)zipping rates $\mathsf{t}^\pm$, we impose the boundary condition

$$\mathsf{r}^+\left(m, n^{\max}(m)\right) = 0, \tag{9}$$

i.e., once the denaturation wedge is completely occupied, no additional SSB is allowed to bind; and when $n = 0$ SSBs are bound, no further SSB can detach:

$$\mathsf{r}^-(m, 0) = 0, \tag{10}$$

The configuration lattice showing the allowed moves is illustrated in figure 3. Empty arrow heads indicate forbidden moves.

The general solution of the master equation (4) can be obtained through the ansatz

$$P(m, n, t) = \sum_p c_p Q_p(m, n)\mathrm{e}^{-\eta_p t}, \tag{11}$$

corresponding to an expansion in eigenmodes. Here, the expansion coefficients c_p are determined by the initial condition. Inserting the above expansion into equation (4) produces

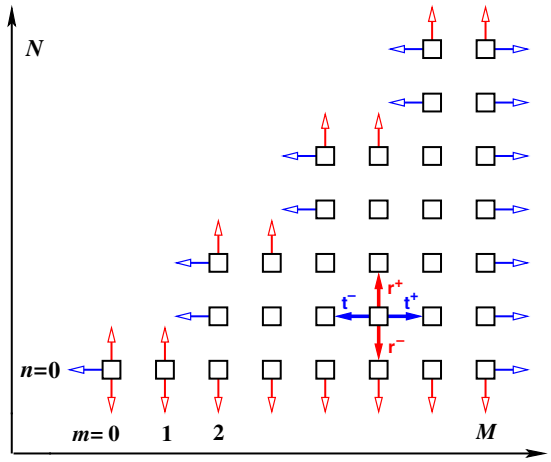

Figure 3. Configuration lattice showing the possible configurations □ of the system in the (m, n)-plane. The empty arrow heads represent forbidden moves due to the boundary conditions. The maximum number of bound SSBs is $N = 2[M/\lambda]$.

the eigenvalue equation

$$\begin{aligned} -\eta_p Q_p(m,n) &= \mathsf{t}^+(m-1,n)Q_p(m-1,n) + \mathsf{t}^-(m+1,n)Q_p(m+1,n) \\ &\quad - [\mathsf{t}^+(m,n) + \mathsf{t}^-(m,n)]Q_p(m,n) \\ &\quad + \mathsf{r}^+(m,n-1)Q_p(m,n-1) + \mathsf{r}^-(m,n+1)Q_p(m,n+1) \\ &\quad - [\mathsf{r}^+(m,n) + \mathsf{r}^-(m,n)]Q_p(m,n) \end{aligned} \tag{12}$$

for the pth eigenmode. The concrete forms for the transfer rates are defined in the next section.

4. Partition function and transfer rates

In order to obtain the transfer coefficients $\mathsf{t}^\pm$ and $\mathsf{r}^\pm$, we first define the partition coefficient $\mathscr{Z}(m,n)$ for the end-denaturation fork of the dsDNA and the SSBs bound to its two branches. To this end, we note that we can decouple the partition coefficient

$$\mathscr{Z}(m,n) = \mathscr{Z}^{\mathrm{DNA}}(m)\mathscr{Z}^{\mathrm{SSB}}(m,n) \tag{13}$$

into the contributions $\mathscr{Z}^{\mathrm{DNA}}$ counting the degrees of freedom of the DNA molecule, and the contribution $\mathscr{Z}^{\mathrm{SSB}}$ of the SSBs. According to the Poland–Scheraga model of DNA denaturation, we have

$$\mathscr{Z}^{\mathrm{DNA}}(m) = u^m. \tag{14}$$

Here, $u = \exp(\beta\epsilon)$ is the Boltzmann factor for opening a base-pair, i.e., the activation needed to overcome the free energy barrier ϵ for opening an additional base-pair. ϵ combines two appreciable contributions from enthalpy cost and entropy gain on breaking the base-pair that almost cancel, such that ϵ is of the order of $k_{\mathrm{B}}T$ at physiological temperature and salt conditions: at 37°, $u \approx 0.6$ in a zone of AT base-pairs, and $u \approx 0.2$ in a GC domain [14]. We note that the parameter u is sensitive to the salt concentration. Here, we consider homopolymer zones of either AT or GC; for the treatment of a heteropolymer, see [20]. As already mentioned, we also neglect the formation of internal denaturation bubbles within the dsDNA stretch that would require the crossing of the initiation barrier σ_0. This contrasts with the situation for our

previous studies [21, 17, 18, 20, 22], in which we focused on internal bubbles, preventing end-denaturation wedges by clamping at both ends. Note also that in the case of the end-wedges, we do not have to take care of the entropy loss due to loop formation that occurs in internal denaturation bubbles.

The contribution from the SSBs has the form

$$\mathscr{Z}^{\mathrm{SSB}}(m,n) = \kappa^n \Omega^{\mathrm{SSB}}(m,n), \tag{15}$$

sharing the energetic component

$$\kappa = c_0 K^{\mathrm{eq}} \tag{16}$$

per bound SSB, where c_0 is the SSB concentration in solution and $K^{\mathrm{eq}} = v_0 \exp(|E_{\mathrm{bind}}|/k_{\mathrm{B}}T)$ the equilibrium binding constant of SSB binding, with the typical volume v_0 of the SSBs and the binding energy E_{bind}; and the number of possible ways of arranging n SSBs on the two arches of the denaturation fork, both of length m [17, 18], is

$$\Omega^{\mathrm{SSB}}(m,n) = \sum_{n'=0}^{n} \omega^{\mathrm{SSB}}(m,n')\omega^{\mathrm{SSB}}(m,n-n') \Big|_{n' \leqslant n^{\max}/2}^{n-n' \leqslant n^{\max}/2}. \tag{17}$$

This counting allows us to have different numbers of SSBs on the two arches. The number of ways of distributing n SSBs each covering λ bases, on an arch of size m, is

$$\omega^{\mathrm{SSB}}(m,n) = \binom{m-(\lambda-1)n}{n} = \frac{(m-[\lambda-1]n)!}{n!(m-\lambda n)!}. \tag{18}$$

From the partition function, we can now specify the transfer rates. As a first requirement we impose that the rates obey the detailed balance condition [23]

$$\mathsf{r}^{+}(m,n-1)\mathscr{Z}(m,n-1) = \mathsf{r}^{-}(m,n)\mathscr{Z}(m,n) \tag{19}$$

for SSB (un)binding and

$$\mathsf{t}^{+}(m-1,n)\mathscr{Z}(m-1,n) = \mathsf{t}^{-}(m,n)\mathscr{Z}(m,n) \tag{20}$$

for base-pair (un)zipping. Detailed balance guarantees that the probability distribution $P(m,n,t)$ for long times relaxes towards the Boltzmann distribution. However, the detailed balance condition does not uniquely specify the rates. Using the remaining freedom of choice [23, 17], we settle for the following forms. In the case of SSB (un)binding, we choose

$$\mathsf{r}^{+}(m,n) = (n+1)q\frac{\mathscr{Z}(m,n+1)}{\mathscr{Z}(m,n)} = (n+1)q\kappa\frac{\Omega^{\mathrm{SSB}}(m,n+1)}{\Omega^{\mathrm{SSB}}(m,n)} \tag{21}$$

for the binding rate and

$$\mathsf{r}^{-}(m,n) = nq \tag{22}$$

for unbinding. The unbinding rate, that is, is proportional to the number of bound SSBs, as it should be. Apart from this n-factor, we choose it to solely depend on the constant unbinding rate q. Conversely, the binding rate includes, apart from this rate q, the binding strength κ, the relative number of degrees of freedom given by the ratio of the Ω^{SSB} factors, and the factor $(n+1)$. The factor $(n+1)\Omega^{\mathrm{SSB}}(m,n+1)/\Omega^{\mathrm{SSB}}(m,n)$ accounts for the combinatorial number of ways to put an additional SSB of size λ onto either arch of the denaturation fork. For $\lambda = 1$ the resulting expression for $\mathsf{r}^{+}(m,n)$ becomes $q\kappa(m-n)$ and thus designates the number of free binding sites; compare the discussion in [17, 23].

Similarly, we choose a completely asymmetric form for the base-pair (un)zipping rates. Thus, for unzipping an additional base-pair we use[1]

$$\mathrm{t}^{+}(m,n) = \mathrm{t}^{+}(m) = k\frac{\mathscr{Z}^{\mathrm{DNA}}(m+1,n)}{\mathscr{Z}^{\mathrm{DNA}}(m,n)} = ku, \tag{23}$$

carrying the full Boltzmann factor u, apart from the rate constant k. The zipping rate

$$\mathrm{t}^{-}(m,n) = k\frac{\mathscr{Z}^{\mathrm{DNA}}(m-1,n)}{\mathscr{Z}^{\mathrm{DNA}}(m,n)} = k\frac{\Omega^{\mathrm{SSB}}(m-1,n)}{\Omega^{\mathrm{SSB}}(m,n)} \tag{24}$$

contains all information related to the interplay with the number m of bound SSBs, and is proportional to the probability that the base-pair next to the denaturation fork is unoccupied. This choice realistically describes the fact that a region almost fully occupied with SSBs is less likely to decrease in size. We note that in general $\mathrm{t}^{-}(m,n) \leqslant k$, and that $\mathrm{t}^{-}(m,0) = k$. Note also that we can conveniently define a dimensionless parameter

$$\gamma \equiv \frac{q}{k} \tag{25}$$

that measures the competition between SSB (un)binding and base-pair (un)zipping.

5. Results: blinking autocorrelation of the molecular beacon

Having defined the dynamics of the end-denaturation wedge in terms of the numbers of broken base-pairs, m, and of bound SSBs, n, we now proceed to calculate the autocorrelation $A(t)$ for the blinking behaviour of a fluorophore–quencher pair mounted on the denaturation wedge as shown in figure 2. Following the results from [20], we can express $A(t)$ according to equation (2) in the form

$$A(t) = \sum_{p\neq 0} T_p^2 \mathrm{e}^{-t/\tau_p}, \tag{26}$$

with relaxation times $\tau_p \equiv \eta_p^{-1}$, and where

$$T_p = \sum_{m,n} Q_p(m,n)\Big|_{m\geqslant x_T}. \tag{27}$$

It should also be noted that, in order to enable experimental detection, it might be necessary for the fluorophore–quencher pair to be separated to more than the separation provided by solely opening the base-pair x_T. Thus, if Δ additional base-pairs need to be broken before fluorescence occurs, the quantity T_p will be modified to $T_p = \sum_{m,n} Q_p(m,n)\big|_{m\geqslant x_T+\Delta}$.

Alternatively, we can rewrite the autocorrelation function $A(t)$ according to the spectral decomposition

$$A(t) = \int_0^\infty f(\tau)\exp\left(-\frac{t}{\tau}\right)\mathrm{d}\tau. \tag{28}$$

In this way, we obtain the weighted spectral density ('relaxation time spectrum')

$$f(\tau) = \sum_{p\neq 0} T_p^2 \delta\left(\tau - \tau_p\right). \tag{29}$$

This distribution $f(\tau)$ yields information about the contributions of individual relaxation modes to the autocorrelation function $A(t)$; see also below.

[1] We here, for simplicity, neglect any m-dependence of the rate constant k; compare the discussion about the 'hook' effect in [17, 18].

For the two limiting cases corresponding to the absence of SSBs and to fast (un)binding dynamics of the SSBs, we obtain analytical solutions for $A(t)$ from the master equation (4) below. The general case is solved numerically along similar lines to what was developed in [17].

5.1. Absence of SSBs

If no SSBs are present, the (un)zipping rates $\mathrm{t}^{\pm}$ assume the simpler form

$$\bar{\mathrm{t}}^{+}(m) = \mathrm{t}^{+}(m,0) = ku, \tag{30}$$

and

$$\bar{\mathrm{t}}^{-}(m) = \mathrm{t}^{+}(m,0) = k, \tag{31}$$

corresponding to the transfer rates for an asymmetric random walk. This contrasts with the non-linear form for internal bubbles, which includes the loop entropy loss [17, 18]. The master equation reduces to the one-variable form

$$\frac{\partial \overline{P}(m,t)}{\partial t} = \bar{\mathrm{t}}^{+}(m-1)\overline{P}(m-1,t) + \bar{\mathrm{t}}^{-}(m+1)\overline{P}(m+1,t) - [\bar{\mathrm{t}}^{+}(m) + \bar{\mathrm{t}}^{-}(m)]\overline{P}(m,t) \tag{32}$$

with the eigenvalue decomposition $\overline{P}(m,t) = \sum_p \bar{c}_p \overline{Q}_p(m)\mathrm{e}^{-\bar{\eta}_p t}$. Thus, we obtain the eigenvalue equation

$$-\bar{\eta}_p \overline{Q}_p(m) = \bar{\mathrm{t}}^{+}(m-1)\overline{Q}_p(m-1) + \bar{\mathrm{t}}^{-}(m+1)\overline{Q}_p(m+1) - [\bar{\mathrm{t}}^{+}(m) + \bar{\mathrm{t}}^{-}(m)]\overline{Q}_p(m), \tag{33}$$

with the obvious boundary conditions $\bar{\mathrm{t}}^{-}(0) = 0$ and $\bar{\mathrm{t}}^{+}(M) = 0$. The solution of the reduced eigenvalue equation for $\overline{Q}_p$ can be obtained in terms of orthogonal polynomials (or Chebyshev polynomials) according to [17, 24]

$$\overline{Q}_p(m) = \frac{u^{m/2}}{\sin\omega_p}\left\{\sin\left[(m+1)\omega_p\right] - u^{-1/2}\sin\left[m\omega_p\right]\right\}, \tag{34}$$

where the eigenvalues become

$$\bar{\eta}_p = k\left[u + 1 - 2u^{1/2}\cos\omega_p\right] \tag{35}$$

with

$$\omega_p = \frac{p\pi}{M+1}. \tag{36}$$

We notice that the relaxation times $\bar{\tau}_p \equiv 1/\bar{\eta}_p$ fulfil the inequalities

$$\tau_{\min}(u) \equiv k^{-1}\left(1+u^{1/2}\right)^{-2} \leqslant \bar{\tau}_p \leqslant k^{-1}\left(1-u^{1/2}\right)^{-2} \equiv \tau_{\max}(u). \tag{37}$$

Thus, at the melting transition where $u = 1$, and for an infinitely long DNA segment $M \to \infty$, the longest relaxation time diverges, i.e., the denaturation wedge has a diverging lifetime, as one would expect. The correlation functions $A(t)$ corresponding to the results above are shown by the black dash–dotted curves in figure 4.

We note that conditions similar to the absence of SSBs are fulfilled if the concentration of SSBs is very low, $\kappa \to 0$, or if $\gamma\kappa \to 0$; compare the existence of a kinetic block to SSB binding in DNA bubbles [2, 3, 17, 18].

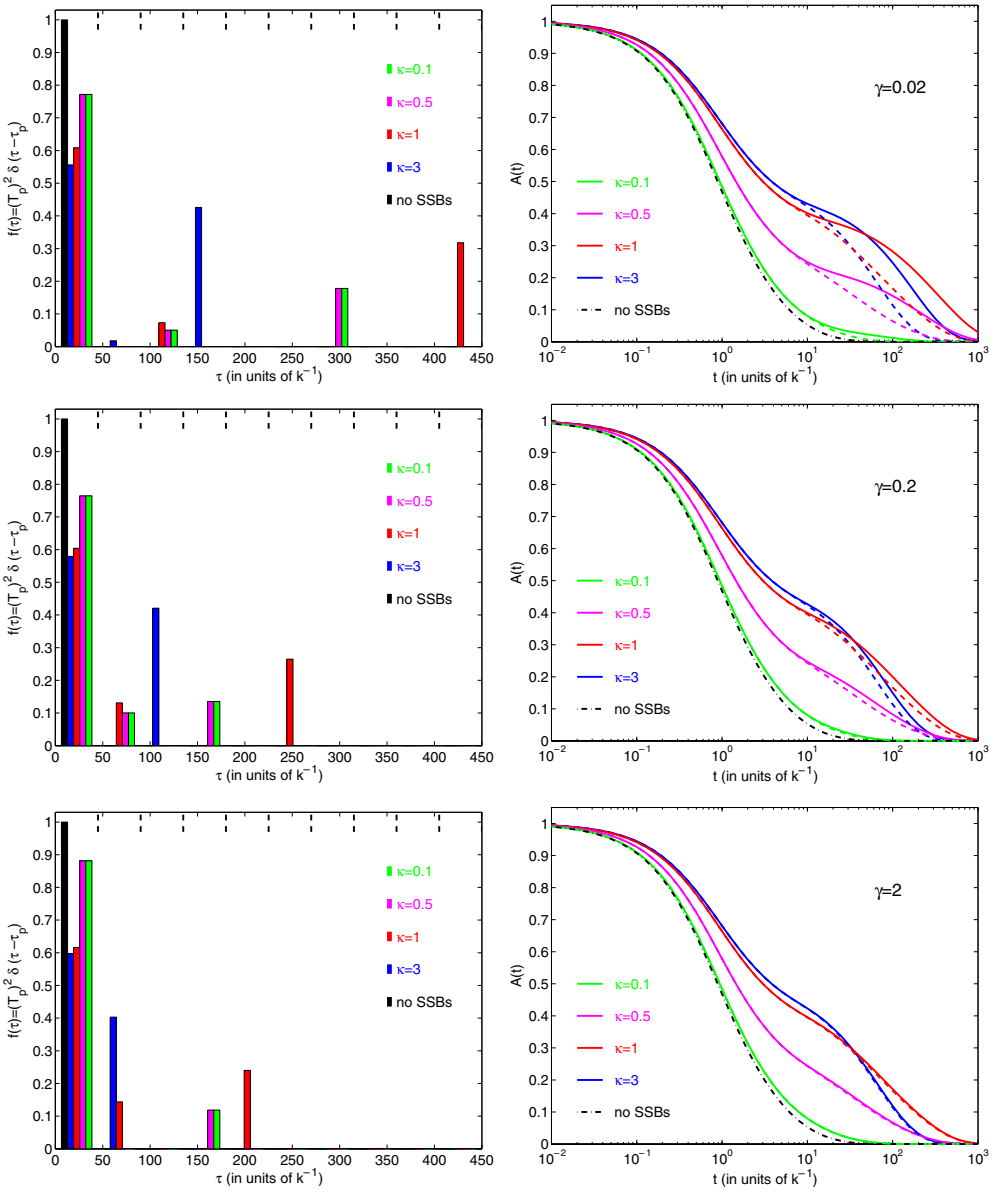

Figure 4. Relaxation time spectrum $f(\tau)$ and autocorrelation function $A(t)$ for different values of the binding strength κ and the ratio $\gamma = q/k$ of the unbinding and the unzipping rate constants, as indicated in the graphs. The dashed curves correspond to the approximation of adiabatic elimination (fast binding). In the plots for the relaxation time spectra, $f(\tau)$, the data were binned (the black dashed lines at the top of the graphs show the bin size). We chose $u = 0.6$, $\lambda = 5$, $x_T = 1$, and $M = 30$. Notice that strongly binding SSBs increase the relaxation time by orders of magnitude (logarithmic abscissa in the $A(t)$ plots).

5.2. Fast (un)binding dynamics of SSBs

In the case where the (un)binding dynamics of the SSBs is much faster than the typical base-pair (un)zipping rates, $\gamma \gg 1$, we can adiabatically eliminate the degrees of freedom corresponding

to the SSB dynamics [25]. Ensuing are an effective free energy landscape, dressed by the SSB interactions with the denaturation wedge, and a reduced one-variable master equation of the type (32), but with the following (dressed) rate coefficients [17]:

$$\tilde{\mathrm{t}}^{\pm}(m) = \sum_{n=0}^{n^{\max}(m)} \mathrm{t}^{+}(m,n)\frac{\mathscr{Z}(m,n)}{\mathscr{Z}(m)}, \tag{38}$$

where $\mathscr{Z}(m) \equiv \sum_n \mathscr{Z}(m,n)$. When calculating the two dressed rates $\tilde{\mathrm{t}}^{\pm}$, it is important to include the boundary conditions (5), (7), and (8). From these we also deduce the modified boundary conditions $\tilde{\mathrm{t}}^{+}(M) = 0$ and $\tilde{\mathrm{t}}^{-}(0) = 0$. The corresponding results for the autocorrelation function are shown by the dashed curves in figure 4.

5.3. General case

In the general case when the dynamics of SSB (un)binding and base-pair (un)zipping occur on comparable timescales, $\gamma \sim 1$, the eigenvalue equation (12) has to be solved numerically; for detailed elaboration of the procedure, see [17]. In figure 4, we display some typical examples for the relaxation time spectrum and the autocorrelation function for various values of the SSB binding strength κ and rate ratio γ.

5.4. Discussion

We first note that the autocorrelation function $A(t)$ in the semi-log plot is non-exponential, corresponding to a multimodal relaxation behaviour that was also observed in experiment [1]. This is reflected in the rather broad distribution of relaxation times shown in figure 4. In the binned data for the relaxation times, the first bin contains the major portion of the relaxation contributions for all cases. This describes the relaxation of the denaturation wedge itself, i.e., the relaxation due to the base-pair (un)zipping process. In the plots for $A(t)$, this corresponds to the first relaxation shoulder located at a few inverse zipping time units, k^{-1}.

In the absence of SSBs, our coarse-grained plot of the relaxation time distribution shows only one contribution, corresponding to only one relaxation shoulder in the graphs for $A(t)$. With increasing binding strength κ, a second relaxation shoulder in $A(t)$ is building up. This is due to the relaxation of SSB (un)binding. Let us discuss the somewhat involved behaviour for the various values of κ in the case of $\lambda = 1$, for which the occupation fraction of SSBs on the ssDNA branches of the denaturation wedge becomes $f = \kappa/(1+\kappa)$ [19]. We see that $\kappa = 1$ leads to an occupation fraction $f = 1/2$. In that case, we would expect the relaxation time for SSB occupation to be the longest. For increasing and decreasing κ, the fractions of vacancies and bound SSBs, respectively, are decreasing, so the exchange between the species becomes faster and $A(t)$ decays quicker than for $\kappa = 1$. However, for $\kappa < 1$, the number of bound SSBs is smaller and mostly a certain binding site is vacant, and the relaxation therefore quicker than for $\kappa > 1$, for which a site is mostly occupied. Indeed, these trends can be observed in the plotted examples. The relaxation time contribution is the longest in the case $\kappa = 1$. This observation is corroborated in figure 5 illustrating the behaviour of the longest relaxation time as a function of the binding strength κ: the maximum close to $\kappa \approx 1$ is distinct.

In the dependence of the ratio $\gamma = q/k$ of the rates q for SSB unbinding and k for base-pair unzipping, the increase in the relative speed, γ, of the SSB dynamics is immediately evident from the shift towards shorter τ in the relaxation time spectrum. In the plots for $A(t)$, the results in the presence of SSBs approach the adiabatic approximation; in the case $\gamma = 2$, virtually no difference between the full result and the fast binding limit are visible in $A(t)$.

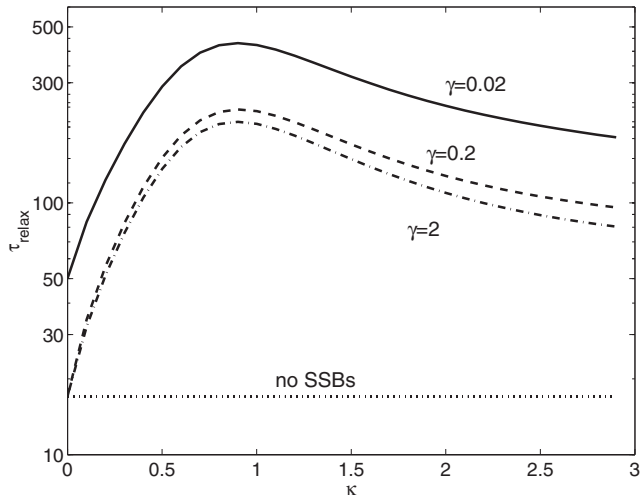

Figure 5. Longest relaxation time $\tau_{\rm relax}$ as a function of SSB binding strength κ. Note the dramatic variation of $\tau_{\rm relax}$ (logarithmic ordinate). We chose $u = 0.6$, $\lambda = 5$, and $M = 30$. A maximum occurs at around $\kappa = 1$.

6. Conclusions

We investigated by means of a master equation approach, in detail, the dynamics of end-denaturation of a clamped stretch of homopolymer DNA. The transfer rates were obtained from the partition coefficients based on the Poland–Scheraga model of DNA denaturation. We chose the rates $t^{\pm}$ and $r^{\pm}$ for base-pair (un)zipping and SSB (un)binding, such that detailed balance is fulfilled, i.e., thermal equilibrium reached for long times. We furthermore chose these rates in a fully asymmetric form, guaranteeing that base-pair unzipping is proportional to the Boltzmann factor for breaking the base-pair and the fundamental rate k. For base-pair zipping, the rate is given by k in the absence of SSBs, whereas in the presence of SSBs it gets dressed with the combinatorial ratio slowing down the zipping when SSBs are bound (essentially, by the probability that the base-pair next to the zipping fork is vacant), and preventing closing of the wedge once it is fully occupied. Similarly, we chose the (un)binding rates such that the unbinding is specified by the fundamental rate q times the number of bound SSBs. Binding is biased by the binding strength κ and the probability of adding another SSB to the two arches of the denaturation wedge.

Mounting a fluorophore–quencher pair at position x_T on either arch of the associated denaturation wedge, a molecular beacon is built whose blinking dynamics, corresponding to the open or closed state of the base-pair x_T, is described by the random variable I. For this quantity, we obtained the autocorrelation function $A(t)$ and the associated spectrum of relaxation times. The quantity $A(t)$ can be measured directly in experiments (see, e.g., [1, 15]). The predicted behaviour of $A(t)$ and the spectrum $f(\tau)$ shows a multimodal behaviour with two pronounced relaxation shoulders in the presence of SSBs. As our model involves physical parameters that are known for given solvent conditions (u, κ) or can be determined independently (k, q), our model becomes fully quantitative, and can be used to devise future experimental set-ups.

The molecular beacon set-up we propose represents the basis for an interesting nanosensor. Constructing a small stretch of AT base-pairs and clamping them with a few GC base-pairs at one end (compare the construction used in [1]), such a nanosensor would be of the linear

size of some 20 nm. A low concentration of such nanosensors would therefore be sufficient to probe for the presence of SSBs, salt conditions, or similar, in small probe volumes such as are encountered in gene arrays. The rather large changes in the relaxation time spectrum invoked by the presence of SSBs (or, by varying u, corresponding to temperature or salt condition changes, not shown here) corroborate that this kind of sensor could actually be rather sensitive. We note that instead of the conventional fluorophores, which bleach rather quickly, longer-lived quantum dots or plasmon resonant nanoparticles are now available; see, for instance, [26, 27].

Whereas our calculations are for a homopolymer denaturation zone, the simplest possibility with a view to designing a nanodevice, it is possible to extend the model to a heterogeneous sequence; see [20]. However, the numerical evaluation of the corresponding master equation may become challenging, especially when longer denaturation zones and small SSBs are employed. An efficient alternative for such more involved cases is provided by stochastic simulations techniques such as the Gillespie algorithm, as studied recently in the context of denaturation fluctuations in DNA [22].

References

[1] Altan-Bonnet G, Libchaber A and Krichevsky O 2003 *Phys. Rev. Lett.* **90** 138101
[2] Pant K, Karpel R L and Williams M C 2003 *J. Mol. Biol.* **327** 571
[3] Pant K, Karpel R L, Rouzina I and Williams M C 2004 *J. Mol. Biol.* **336** 851
[4] Rief M, Gautel M, Oesterhelt F, Fernandez J M and Gaub H E 1997 *Science* **276** 1109
[5] Kasianowicz J J, Brandin E, Branton D and Deamer D W 1996 *Proc. Natl Acad. Sci. USA* **93** 13770
[6] Meller A 2003 *J. Phys.: Condens. Matter* **15** R581
[7] Liphardt J, Dumont S, Smith S B, Tinoco I Jr and Bustamante C 2002 *Science* **296** 1832
[8] Jarzynski C 1997 *Phys. Rev. Lett.* **78** 2690
[9] Seifert U 2005 *Phys. Rev. Lett.* **95** 040602
[10] Lehn J-M 1995 *Supramolecular Chemistry* (Weinheim: Wiley–VCH)
[11] Hanke A and Metzler R 2003 *Chem. Phys. Lett.* **359** 22
[12] Bottari G, Dehez F, Leigh D A, Nash P J, Perez E M, Wong J K Y and Zerbetto F 2003 *Angew. Chem. Int. Edn* **42** 5886
[13] Ambjörnsson T and Metzler R 2005 *J. Comput. Theor. Nanosci.* at press
[14] Blake R D, Bizzaro J W, Blake J D, Day G R, Delcourt S G, Knowles J, Marx K A and SantaLucia J Jr 1999 *Bioinformatics* **15** 370
[15] Krichevsky O and Bonnet G 2002 *Rep. Prog. Phys.* **65** 251
[16] Sokolov I M, Metzler R, Pant K and Williams M C 2005 *Biophys. J.* **89** 895
[17] Ambjörnsson T and Metzler R 2005 *J. Phys.: Condens. Matter* **17** S1841
[18] Ambjörnsson T and Metzler R 2005 *Phys. Rev.* E at press
[19] Ambjörnsson T and Metzler R 2004 *Phys. Biol.* **1** 77
[20] Ambjörnsson T and Metzler R 2005 in preparation
[21] Hanke A and Metzler R 2003 *J. Phys. A: Math. Gen.* **36** L473
[22] Banik S K, Ambjörnsson T and Metzler R 2005 *Europhys. Lett.* **71** 852
[23] van Kampen N G 1992 *Stochastic Processes in Physics and Chemistry* (Amsterdam: North-Holland)
[24] Ledermann W and Reuter G E H 1954 *Phil. Trans. R. Soc.* A **246** 321
[25] Risken H 1989 *The Fokker–Planck Equation* (Berlin: Springer)
[26] Medintz I L, Clapp A R, Mattoussi H, Goldman E R, Fisher B and Mauro J M 2003 *Nat. Mater.* **2** 630
[27] Shultz D A 2003 *Curr. Opin. Biotechnol.* **14** 13